ELSEVIER

Fluid Dynamics Research 17 (1995) 67–85

FLUID DYNAMICS RESEARCH

An optimal theory for an expansion of flow quantities to capture the flow structures ★

The remainder minimization method in the Sobolev space $W^{m,p}(\Omega_T)$

Chui-Jie Wu, Han-Sheng Shi

Laboratory for Nonlinear Mechanics of Continuous Media, Institute of Mechanics, Academia Sinica of China, Beijing 100080, China

Air Force Institute of Meteorology, Nanjing, 21101, China

Received 5 December 1994; revised 27 March 1995

Abstract

An optimal theory on flow database analysis to capture the flow structures has been developed in this paper, which include the POD method as its special case. By means of the remainder minimization method in the Sobolev space, for more general optimal conditions the new theory has the potential to overcome an inherent limitation of the POD method, i.e., it cannot be used to the situations in which the optimal condition is other than the inner product global one. As an example, using the new theory, the database of a two-dimensional flow over a backward-facing step is analyzed in detail, with velocity and vorticity bases.

1. Introduction

Turbulence is one of the most difficult and unsolved problems in classical physics. The studies of coherent structures of turbulence are the keys to understanding the physical essence of turbulence. The primary question to address is: how to objectively understand and analyze coherent structures in order to reveal the physical character of turbulence. From published literature (see Berkooz et al. (1993) or Wu and Shi (1994) and the references therein) it can be found that the POD method (proper orthogonal decomposition) played an important role.

The history of the POD method (or the Karhunen–Loéve procedure) can be traced back to Schmidt (1907) [1]. Now there are several extensions to the POD, such as the snapshot form of the POD (Sirovich, 1987), EPOD (Glezer et al., 1989) and Kirby's extension. By applying the

★ This project is supported by the National Natural Science Foundation of China # 19472077.

[1] We are grateful to Professor Sirovich for pointing out this fact.

SSDI 0169-5983(95)00024-0

weighted Sobolev norm, Kirby optimized the approximation of the higher derivative terms in numerical simulations of PDE, and reduced the size of the associated systems of ODE. The goal of Kirby's (1992) extension is to minimize $\langle w_0|u-u^N|^2+w_1|u_x-u_x^N|^2+w_2|u_{xx}-u_{xx}^N|^2+\cdots\rangle$, which is a kind of global inner product optimal condition.

It should be noted that the POD method or its extensions cannot be used for the situations in which the optimal conditions are other than the inner product global ones. Sometimes the most essential characters of the system are unable to be presented by the optimal condition of global inner product, and with such optimal conditions it is impossible to focus one's attention on some key region, such as the production of vorticity on the boundaries, or to accurately describe some important flow phenomena in a certain time period, such as the breakdown of vortices.

The work presented here puts forward an optimal theory for an expansion of flow quantities to capture the flow structures, which can overcome the above mentioned shortcoming and is a part of the general optimal theory on flow database analysis and construction of low-dimensional dynamical systems (Wu and Shi, 1994). The new theory has the potential to extract predetermined flow structures, with various spatiotemporal and local-global optimal conditions.

The paper is organized as follows. In Section 2 we outline the optimal theory on flow database analysis. In Section 3 we apply the theory to the standard backward facing step flow, and compare two different optimal conditions and sets of optimal bases. Finally, in Section 4 we arrive at some conclusions.

2. The optimal theory on flow database analysis

In order to find organized motions in a given set of realizations of a random field, Lumly (1967) first introduced the POD method into the studies of turbulence. The applications of this method are limited to certain types of flows in which large coherent structure contain a major fraction of the energy. But such "structures" are quite different from the coherent structures observed in experiments. The basic reason is that often the coherent structures found in experiments are not the structures which contain most energy. Therefore it is necessary to develop a new method by which the various flow features, not only in the sense of quadratic mean, can be optimally extracted from flow databases.

2.1. Theory

The basic idea of the new theory is, using the method of optimal control theory, to find the optimal orthogonal bases $\boldsymbol{\xi}_i$ from flow databases $\boldsymbol{u}(\boldsymbol{x},t)$, which are entirely depended on the optimal condition. For the same database, with different optimal conditions, i.e., different characters to be extracted, different optimal bases can be found. Next we will develop the theory in real space, but it can be readily extended into complex space.

For a known flow database $\boldsymbol{u}(\boldsymbol{x},t)$, in which $\boldsymbol{x}\in\Omega\subset\mathcal{R}^n, t\in[0,T]$, and T is a fixed time, suppose $\boldsymbol{u}(\boldsymbol{x},t)$ satisfies

$$\boldsymbol{u}(\boldsymbol{x},t)\in\mathcal{W}^{m,p}(\Omega_T), \tag{2.1}$$

where the indices m, p are related to the smoothness of the flow field $\boldsymbol{u}$, $p=2q; m,q\in\mathcal{N},\mathcal{N}$ is the set of all positive integers, $\Omega_T=[0,T]\times\Omega, \mathcal{W}^{m,p}(\Omega_T)$ is a Sobolev space, in which the norm is

defined as

$$\|\boldsymbol{u}\|_{\mathcal{W}^{m,p}(\Omega_T)} = \left(\sum_{|\alpha| \le m} \|D^{\alpha}\boldsymbol{u}\|^{p}_{\mathcal{L}^{p}(\Omega_T)} \right)^{1/p}, \tag{2.2}$$

where D^{α} is the generalized derivative with index α, $\mathcal{L}^{p}(\Omega_T)$ is the set of all pth integrable functions in Ω_T. If $v = (v_1, \cdots, v_n)^T \in \mathcal{L}^{p}(\Omega_T)$; then

$$\|\boldsymbol{v}\|_{\mathcal{L}^{p}(\Omega_T)} = \left(\int_{\Omega_T} \sum_{i=1}^{n} v_i^{p} \, \mathrm{d}\boldsymbol{x} \, \mathrm{d}t \right)^{1/p}. \tag{2.3}$$

Select a positive integer N, define a functional space $\mathcal{B}_N$

$$\mathcal{B}_N \triangleq \left\{ \xi = (\boldsymbol{\xi}_1(\boldsymbol{x}), \cdots, \boldsymbol{\xi}_N(\boldsymbol{x}))^T \mid \boldsymbol{x} \in \Omega \subset \mathcal{R}^n, \xi \in \mathcal{W}^{m,p}(\Omega), (\boldsymbol{\xi}_i, \boldsymbol{\xi}_j) = \delta_{ij} \right\}, \tag{2.4}$$

where $(\cdot, \cdot)$ is the inner product in the Hilbert space $\mathcal{L}^2(\Omega)$, i.e., if $\boldsymbol{a}, \boldsymbol{b} \in \mathcal{L}^2(\Omega)$, then $(\boldsymbol{a}, \boldsymbol{b}) = \int_{\Omega} \boldsymbol{a} \cdot \boldsymbol{b} \, \mathrm{d}\boldsymbol{x}$. We make the following decomposition:

$$\boldsymbol{u}(\boldsymbol{x}, t) = \sum_{i=1}^{N} a_i(t)\boldsymbol{\xi}_i(\boldsymbol{x}) + \boldsymbol{u}_R(\boldsymbol{x}, t), \quad \boldsymbol{\xi}_i \in \mathcal{B}_N, \tag{2.5}$$

where $\boldsymbol{u}_R$ is the remainder, and $a_i(t)$ satisfies

$$a_i(t) = (\boldsymbol{u}, \boldsymbol{\xi}_i). \tag{2.6}$$

Since the POD method is based on the concepts of global means of space and time, it is hard to faithfully represent the local structures of the flow. Here we want to keep $\sup_{(x,t)\in\Omega_T} | \boldsymbol{u}_R |$ under control, hence make sure the local features of the flow will be reflected in the optimal bases. The Sobolev embedding theorem ensures this can be achieved, i.e., if Ω_T is a region with cone property in $\mathcal{R}^n$, $\boldsymbol{u}_R \in \mathcal{W}^{m,p}(\Omega_T)$, $mp > n$, then there exists an embedding constant $c(\Omega_T)$, which is only related to region Ω_T, such that $\sup_{(x,t)\in\Omega_T} | \boldsymbol{u}_R(\boldsymbol{x}, t) | \le c(\Omega_T)\|\boldsymbol{u}_R\|_{\mathcal{W}^{m,p}(\Omega_T)}$. Therefore in order to put $\sup_{(x,t)\in\Omega_T} | \boldsymbol{u}_R(\boldsymbol{x}, t) |$ under control, we only need to minimize $\|\boldsymbol{u}_R\|_{\mathcal{W}^{m,p}(\Omega_T)}$. For the details of the Sobolev space and the complete form of the Sobolev embedding theorem, the reader is referred to Adams (1975).

For the purpose of minimizing the norm of the remainder $\boldsymbol{u}_R(\boldsymbol{x}, t)$ in the Sobolev space, we construct the function of optimal condition as

$$J(\boldsymbol{u}_R) = J(\xi) = \|\boldsymbol{u}_R\|_{\mathcal{W}^{m,p}(\Omega_T)} = \left\| \boldsymbol{u}(\boldsymbol{x}, t) - \sum_{i=1}^{N} a_i(t)\boldsymbol{\xi}_i(\boldsymbol{x}) \right\|_{\mathcal{W}^{m,p}(\Omega_T)}. \tag{2.7}$$

Then the analysis of flow database is converted to the following mathematical problem: find

$$\xi^*(\boldsymbol{x}) = (\boldsymbol{\xi}_1^*(\boldsymbol{x}), \cdots, \boldsymbol{\xi}_N^*(\boldsymbol{x}))^T \in \mathcal{B}_N, \tag{2.8}$$

such that

$$J(\xi^*(\boldsymbol{x})) = \min_{\xi \in \mathcal{B}_N} J(\xi(\boldsymbol{x})), \tag{2.9}$$

where $a_i(t)$ satisfies

$$a_i(t) = (\boldsymbol{u}, \boldsymbol{\xi}_i), \tag{2.10}$$

and $\xi^*(\boldsymbol{x})$ are called the optimal bases of the flow database in the Sobolev space $\mathcal{W}^{m,p}(\Omega_T)$. The above problem can be solved by using the numerical methods of optimal control theory, such as the method of conjugate gradients (Ye and Wang, 1986). In order to compare the new theory with the POD method, here we only consider the case of $m = 0$, $p = 2$; for other situations the numerical procedures and the results will be published elsewhere.

For the case of $m = 0$, $p = 2$, the optimal control condition $J(\xi)$ is an inner product global one, i.e.,

$$J(\xi) = \int_0^T (\boldsymbol{u}, \boldsymbol{u})\, \mathrm{d}t - \int_0^T \sum_{i=1}^N a_i^2(t)\, \mathrm{d}t, \qquad T \text{ fixed}. \tag{2.11}$$

Corresponding to (2.8)–(2.10), the problem becomes: find $\xi^*(\boldsymbol{x}) \in \mathcal{B}_N$, such that

$$J(\xi^*(\boldsymbol{x})) = \max_{\xi \in \mathcal{B}_N} \int_0^T \sum_{i=1}^N a_i^2(t)\, \mathrm{d}t, \tag{2.12}$$

where $a_i(t)$ satisfies

$$a_i(t) = (\boldsymbol{u}, \boldsymbol{\xi}_i), \quad i = 1, \cdots, N. \tag{2.13}$$

Hence, we construct the generalized optimal condition as

$$J^g(\boldsymbol{\xi}_1, \cdots, \boldsymbol{\xi}_N) = \int_0^T \left\{ -\sum_{i=1}^N a_i^2(t) + \sum_{i=1}^N \lambda_i [(\boldsymbol{u}, \boldsymbol{\xi}_i) - a_i] \right\} \mathrm{d}t + \sum_{i,j=1,\ i \le j}^N \lambda_{ij}((\boldsymbol{\xi}_i, \boldsymbol{\xi}_j) - \delta_{ij}), \tag{2.14}$$

where λ_i, λ_{ij} are Lagrangian multipliers. According to the variational method, there must be

$$\delta J^g = 0, \tag{2.15}$$

or

$$\delta J^g = \int_0^T \left(-\sum_{i=1}^N 2a_i \delta a_i + \sum_{i=1}^N \lambda_i \delta a_i \right) \mathrm{d}t + \sum_{i=1}^N \left(\int_0^T \lambda_i \boldsymbol{u}\, \mathrm{d}t, \delta \boldsymbol{\xi}_i \right) + \sum_{i=1}^N \left(\sum_{j=1}^N \tilde{\lambda}_{ij}\, \boldsymbol{\xi}_j, \delta \boldsymbol{\xi}_i \right) = 0, \tag{2.16}$$

where

$$\tilde{\lambda}_{ij} = \begin{cases} 2\lambda_{ij}, & i = j \\ \lambda_{ij}, & i < j \\ \lambda_{ji}, & i > j. \end{cases} \tag{2.17}$$

We choose

$$\lambda = 2a_i; \tag{2.18}$$

then, from (2.16), we get

$$\sum_{j=1}^{N} \tilde{\lambda}_{ij}\, \boldsymbol{\xi}_j + \int_0^T \lambda_i \boldsymbol{u}\, \mathrm{d}t = 0, \qquad i = 1, \cdots, N. \tag{2.19}$$

Using (2.18) in (2.19), then

$$\sum_{j=1}^{N} \tilde{\lambda}_{ij}\, \boldsymbol{\xi}_j + 2\int_0^T a_i \boldsymbol{u}\, \mathrm{d}t = 0. \tag{2.20}$$

Putting the above results together, we have

$$\sum_{j=1}^{N} \tilde{\lambda}_{ij}\, \boldsymbol{\xi}_j + 2\int_0^T a_i \boldsymbol{u}\, \mathrm{d}t = 0, \qquad a_i = (\boldsymbol{u}, \boldsymbol{\xi}_i), \qquad (\boldsymbol{\xi}_i, \boldsymbol{\xi}_j) = \delta_{ij}. \tag{2.21}$$

Applying the orthogonal property of $\boldsymbol{\xi}_i$, the terms of $\tilde{\lambda}_{ij}$ in (2.21) can be found to be

$$\tilde{\lambda}_{ij} = -2\int_0^T a_i a_j\, \mathrm{d}t. \tag{2.22}$$

Using (2.22) in the first equation of (2.21), finally, we arrive at

$$\sum_{j=1}^{N}\left(\int_0^T a_i a_j\, \mathrm{d}t\right)\boldsymbol{\xi}_j = \int_0^T a_i \boldsymbol{u}\, \mathrm{d}t, \qquad i = 1, \cdots, N. \tag{2.23}$$

As one of the referees pointed out, "If (2.13) is substituted into (2.11) and the variation taken, then the usual integral equation (Sirovich, 1987) results". Therefore for the case of $m = 0$, $p = 2$, we recover the POD method; i.e., it reduces to simply another Karhunen–Loéve derivation. Hence, under the optimal condition of global inner product the new theory and the POD method are completely equivalent. But it must be pointed out with emphasis that for the general situation, where $m \neq 0$, $p \neq 2$, the new theory can deal with much wider problems than the POD can, and hence needs further explorations in the future.

2.2. *Numerical procedures*

Instead of the method of conjugate gradients, here the method of direct iteration is used to solve (2.23). Since

$$\boldsymbol{u} = \boldsymbol{u}_{R_0} = a_1 \boldsymbol{\xi}_1 + \boldsymbol{u}_{R_1}, \qquad \boldsymbol{u}_{R_i} = \boldsymbol{u}_{R_{i-1}} - a_i \boldsymbol{\xi}_i = a_{i+1}\boldsymbol{\xi}_{i+1} + \boldsymbol{u}_{R_{i+1}}. \tag{2.24}$$

The following iteration algorithm is used to find $\boldsymbol{\xi}_i$ one by one, associated with (2.24) .

$$a_i^{(k+1)}(t) = \left(\int_\Omega \boldsymbol{u}_{R_i} \cdot \left(\int_0^T a_i^{(k)} \boldsymbol{u}_{R_i}\, \mathrm{d}t\right) \mathrm{d}\boldsymbol{x}\right)\left[\int_\Omega \left(\int_0^T a_i^{(k)} \boldsymbol{u}_{R_i}\, \mathrm{d}t\right)^2 \mathrm{d}\boldsymbol{x}\right]^{-1/2} \tag{2.25}$$

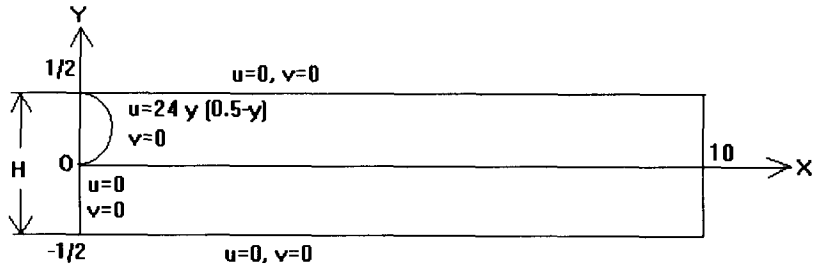

Fig. 1. Standard step flow

and

$$\xi_i = \left(\int_0^T a_i \boldsymbol{u}_{R_i}\,\mathrm{d}t\right)\left(\int_0^T a_i^2\,\mathrm{d}t\right)^{-1}, \tag{2.26}$$

where k is the cyclic index. In the iteration process the following convergent condition is used:

$$\left\| \frac{a_i^{(k)} - a_i^{(k+1)}}{a_i^{(k)}} \right\| < \epsilon, \tag{2.27}$$

where ϵ is a predetermined small parameter, typically 10^{-8}. This iteration algorithm is not sensitive to the initial guess of $a_i^{(0)}$. After the optimal bases have been obtained, they are reordered in the descending sequence according to the amounts of energy contained in them.

3. An example. A two-dimensional backward-facing step flow

In this section, we first numerically solve a two-dimensional backward-facing step flow to get the databases, then apply the new theory developed in Section 2 to examine them.

3.1. Physical model, numerical method and the results of simulations

3.1.1. Physical model

The standard backward facing step flow (Gresho et al., 1990) in two-dimensional incompressible viscous flow field was chosen to be the physical model, as in Fig. 1.

The control equations of two-dimensional incompressible flow are the non-dimensional Navier–Stokes equations and the continuative equation

$$\frac{\partial \boldsymbol{u}}{\partial t} + \boldsymbol{u}\cdot\nabla\boldsymbol{u} = -\nabla p + \frac{1}{\mathrm{Re}}\nabla^2\boldsymbol{u}, \qquad \nabla\cdot\boldsymbol{u} = 0. \tag{3.1}$$

The boundary conditions are as follows, at the inlet boundary $x = 0, 0 \le y \le 0.5$, the velocity is

$$u = 24y(0.5 - y), \qquad v = 0. \tag{3.2}$$

The upper and lower boundaries and the one at $x = 0, -0.5 \le y \le 0$ are solid walls, where the non-slip boundary conditions are applied, i.e.,

$$u = 0, \qquad v = 0. \tag{3.3}$$

The right boundary is continuative outflow boundary. Other geometrical parameters are indicated in Fig. 1. The Reynolds number is defined as

$$\mathrm{Re} = u_{avg} H/\nu, \tag{3.4}$$

where $u_{avg} = 1.0$, H is the distance between the upper and the lower boundaries, ν is the kinematic viscosity of fluid. For the given velocity distribution, it is ease to find that $u_{\max} = 1.5$.

3.1.2. Numerical method

It is necessary to point out that since the main task of this paper is to develop a method to extract optimal orthogonal bases from known databases, then the differences between the data and the true solutions of the problem will not influence the process. Therefore, the principle of choosing the numerical method is to select a mature and reliable algorithm. The finite difference method based on MAC (Marker–and–Cell) algorithm is chosen to numerically solve the two-dimensional Navier–Stokes equations. In the simulation, we use sufficiently refined grids to accurately simulate the flow field. The effective grids in x direction are 200 with $\triangle x = 0.05$, and the effective grids in y direction are 40 with $\triangle y = 0.025$; the time step is 0.005. With the above parameters, stability of computation is ensured.

3.1.3. The results of simulations

Here, we simulate the flow with Re = 700. The most significant character of this flow is that there are two large vortices near the upper and lower parts of the field, respectively, and some smaller vortices around them. The numerical results show that at the starting stage a vortex is produced from the rear part of the step, and moved with the flow down to the exit; at the same time, there is an opposite vortex generated near the upper boundary. It is known from the benchmark solution derived by Gartling (1990) that when the flow reach the stable stage, for Re = 800, the position of reattachment point is approximately at $x = 12$ step heights. For Re = 700, we found that the position of stable reattachment point is at $x = 11.2$ step heights. Hence, when using refined grids the algorithm is feasible and the simulation results are reliable.

3.2. Extraction of the optimal bases from the flow databases

The obtained velocity fields $\boldsymbol{u}(\boldsymbol{x}, t)$ and the vorticity fields $\boldsymbol{\omega}(\boldsymbol{x}, t) = \nabla \times \boldsymbol{u}$ are studied using the numerical procedures described in Subsection 2.2. When dealing with the velocity fields, we take velocity $\boldsymbol{u}$ as the system variable to extract the structures which contain most kinetic energy. Correspondingly, the optimal condition is

$$J(\boldsymbol{\xi}_1^*, \cdots, \boldsymbol{\xi}_N^*) = \max_{(\boldsymbol{\xi}_1^*, \cdots, \boldsymbol{\xi}_N^*) \in \mathcal{B}_N} \int_0^T \sum_{i=0}^{N} a_i^2(t)\, \mathrm{d}t, \tag{3.5}$$

where $a_i(t) = (\boldsymbol{u}, \boldsymbol{\xi}_i)$; the optimal bases $\boldsymbol{\xi}_i$ for these cases are called the optimal velocity bases.

When examining the vorticity fields $\boldsymbol{\omega}$, the purpose is to find the structures which capture most of enstrophy $En = \int_\Omega \boldsymbol{\omega} \cdot \boldsymbol{\omega}\, \mathrm{d}\boldsymbol{x}$; then the vorticity $\boldsymbol{\omega}$ is taken to be the system variable. The form of

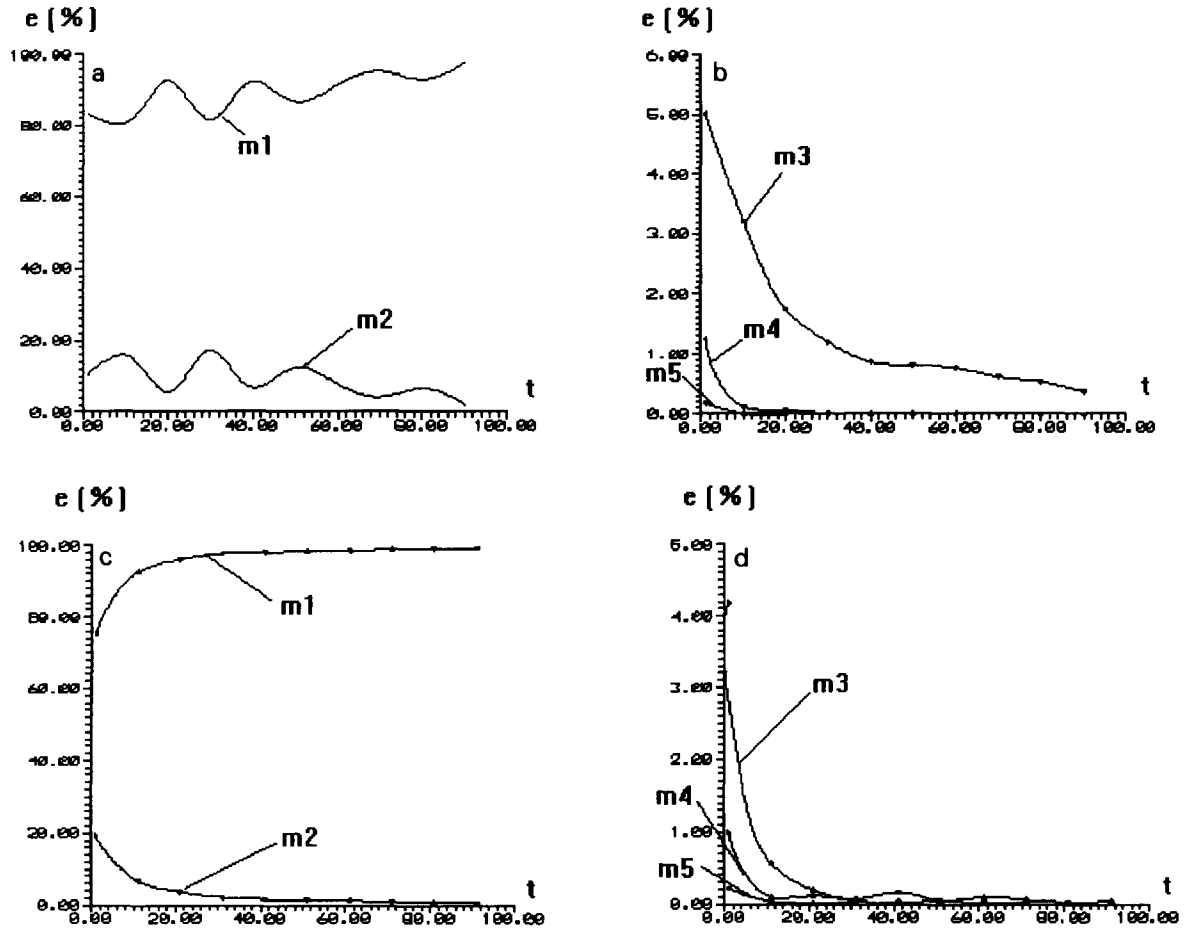

Fig. 2. Time histories of the kinetic energy or the enstrophy contained in the first five modes (a). Time history of the kinetic energy contained in velocity mode 1, 2. (b). Time history of the kinetic energy contained in velocity mode 3, 4, 5. (c). Time history of the enstrophy contained in velocity mode 1, 2. (d). Time history of the enstrophy contained in velocity mode 3, 4, 5.

the optimal condition is the same as (3.5), but now $a_i(t)$ are defined as $a_i(t) = (\omega, \xi_i)$. Hence the optimal bases ξ_i for the vorticity fields are called the optimal vorticity bases.

3.3. The optimal bases and their characteristics

The time histories of the optimal bases, from the starting stage to the quasi-steady stage, have been studied. It is shown that the new theory can be applied to very different flow situations, from the strong unsteady case to the quasi-steady one. In each case, using the optimal velocity bases and the optimal vorticity bases, the effects of kinetic energy and enstrophy in the extraction of characters of flow field have been discussed.

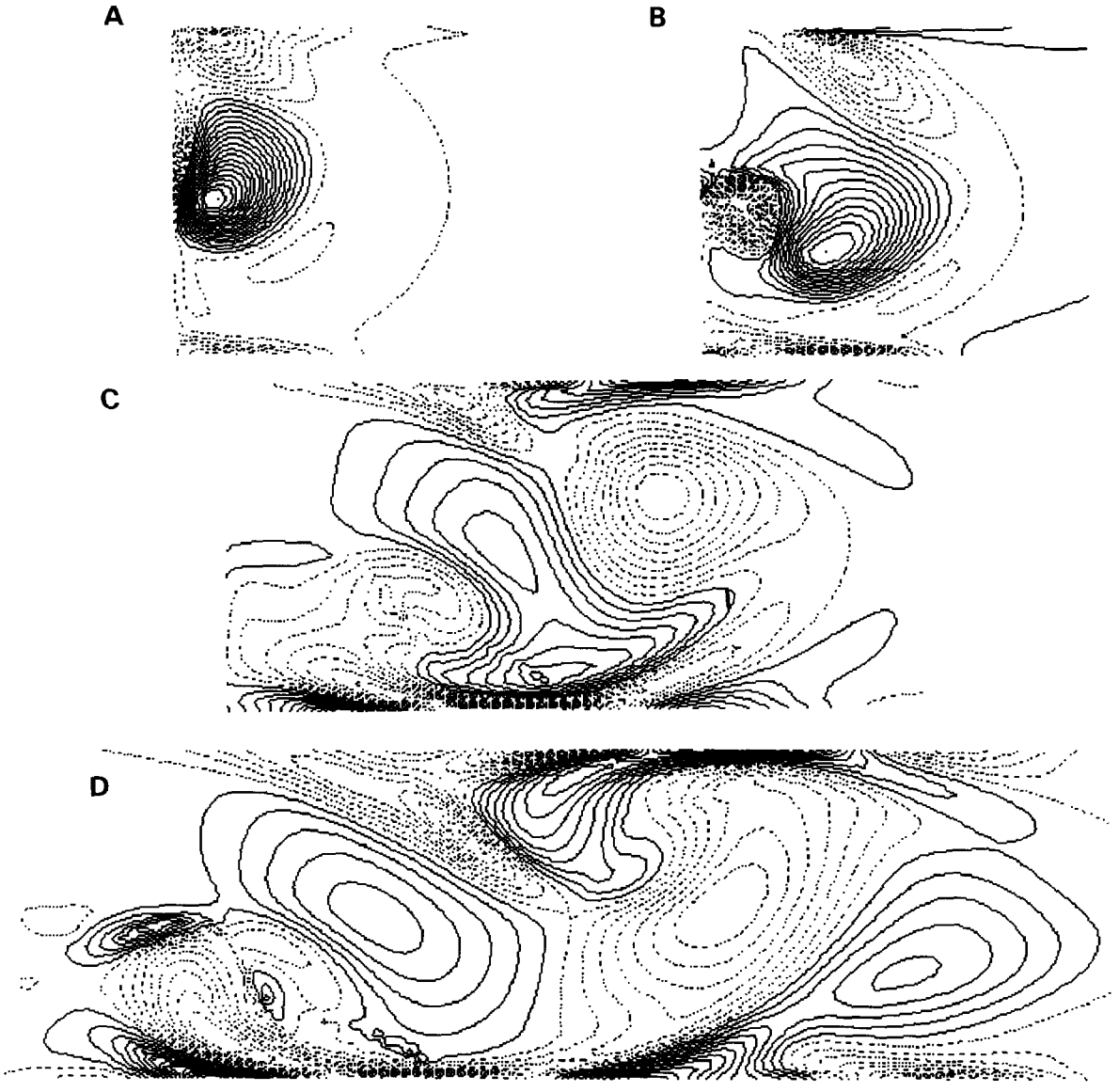

Fig. 3. Equal vorticity counters of the first velocity mode for $t = 1 \sim 110$ (a) $\omega_{max} = 0.7498, \omega_{min} = -0.4058, \Delta\omega = 0.0385, t = 1 \sim 10$ (b) $\omega_{max} = 0.3784, \omega_{min} = -0.4650, \Delta\omega = 0.0281, t = 11 \sim 20$ (c) $\omega_{max} = 0.2233, \omega_{min} = -0.3619, \Delta\omega = 0.0195, t = 21 \sim 30$ (d) $\omega_{max} = 0.1785, \omega_{min} = -0.3148, \Delta\omega = 0.0165, t = 31 \sim 40$ (e) $\omega_{max} = 0.1683, \omega_{min} = -0.2157, \Delta\omega = 0.0128, t = 41 \sim 50$ (f) $\omega_{max} = 0.1449, \omega_{min} = -0.1391, \Delta\omega = 0.0095, t = 51 \sim 60$ (g) $\omega_{max} = 0.1372, \omega_{min} = -0.1029, \Delta\omega = 0.0080, t = 61 \sim 70$ (h) $\omega_{max} = 0.1389, \omega_{min} = -0.0910, \Delta\omega = 0.0077, t = 71 \sim 80$ (i) $\omega_{max} = 0.1408, \omega_{min} = -0.0873, \Delta\omega = 0.0076, t = 81 \sim 90$ (j) $\omega_{max} = 0.1375, \omega_{min} = -0.0914, \Delta\omega = 0.0076, t = 91 \sim 100$ (k) $\omega_{max} = 0.1283, \omega_{min} = -0.0941, \Delta\omega = 0.0074, t = 101 \sim 110$

3.3.1. The optimal velocity bases

Since in both x and y directions the flows are quite inhomogeneous, we expand both directions with the optimal bases. As with the POD method, we only need to decompose the fluctuation parts of the flow field. The time histories of energy distributions $e(\%)$ of first five bases are shown in Fig.

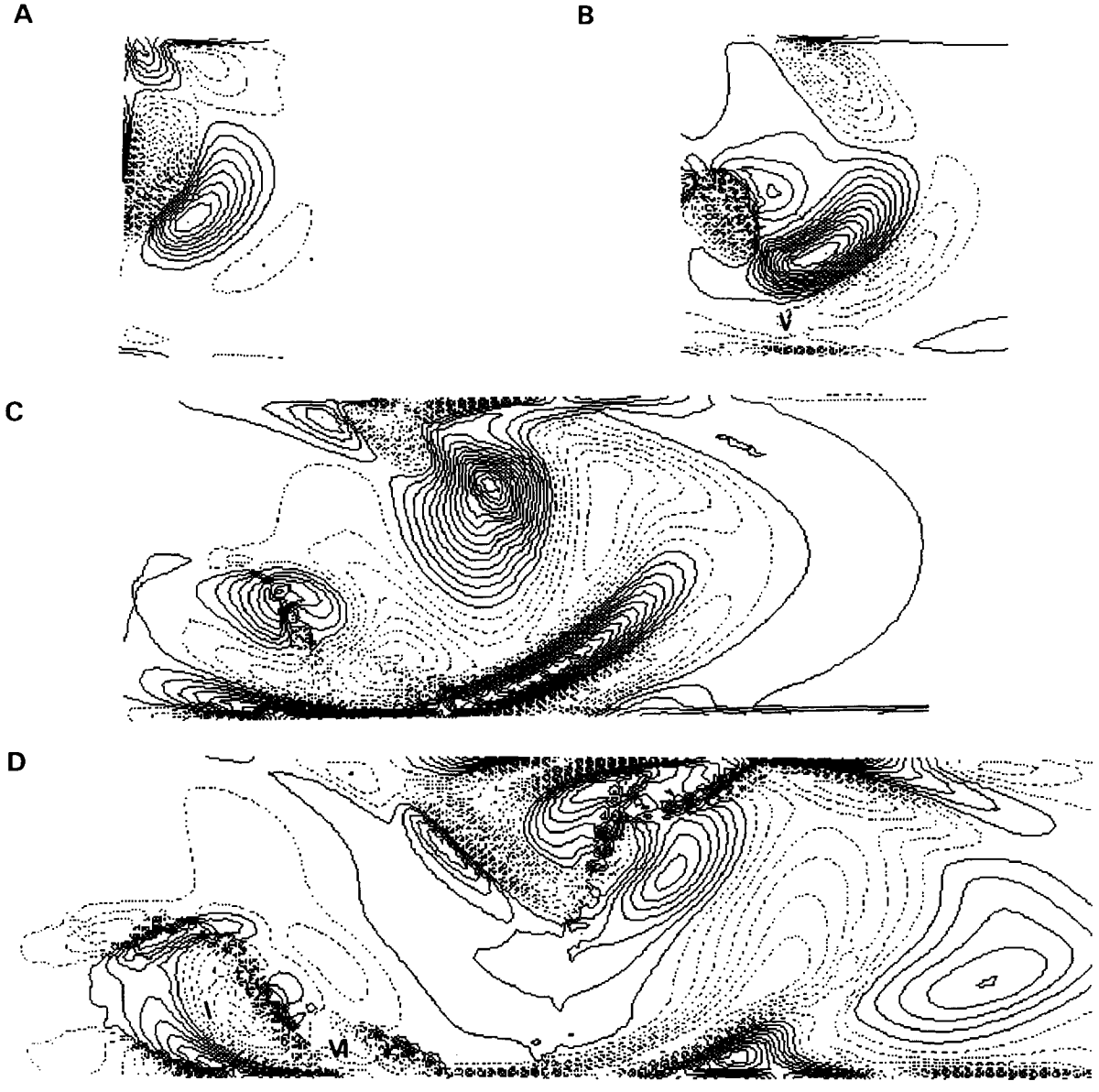

Fig. 4. Equal vorticity counters of the second velocity mode for t =1∼110 (a) $\omega_{max} = 0.2234, \omega_{min} = -0.5288, \Delta\omega = 0.0251, t = 1 \sim 10$ (b) $\omega_{max} = 0.0176, \omega_{min} = -0.0214, \Delta\omega = 0.0013, t = 11 \sim 20$ (c) $\omega_{max} = 0.0416, \omega_{min} = -0.0299, \Delta\omega = 0.0024, t = 21 \sim 30$ (d) $\omega_{max} = 0.0070, \omega_{min} = -0.0108, \Delta\omega = 0.0006, t = 31 \sim 40$ (e) $\omega_{max} = 0.0088, \omega_{min} = -0.0070, \Delta\omega = 0.0005, t = 41 \sim 50$ (f) $\omega_{max} = 0.0032, \omega_{min} = -0.0028, \Delta\omega = 0.0002, t = 51 \sim 60$ (g) $\omega_{max} = 0.0031, \omega_{min} = -0.0029, \Delta\omega = 0.0002, t = 61 \sim 70$ (h) $\omega_{max} = 0.0047, \omega_{min} = -0.0046, \Delta\omega = 0.0003, t = 71 \sim 80$ (i) $\omega_{max} = 0.0014, \omega_{min} = -0.0010, \Delta\omega = 0.0001, t = 81 \sim 90$ (j) $\omega_{max} = 0.0029, \omega_{min} = -0.0037, \Delta\omega = 0.0002, t = 91 \sim 100$ (k) $\omega_{max} = 0.0015, \omega_{min} = -0.0019, \Delta\omega = 0.0001, t = 101 \sim 110$

2. For the starting stage, with the first mode 83.0225% of the total energy has been comprised, and the first four modes collectively contain more than 99.7% of the energy of the motion. Thus even in strong unsteady flows, with just a few modes the new method can still capture most energy of the motion. From Fig. 2, it is obvious that as the flow approaches the steady state, the energy transfers to

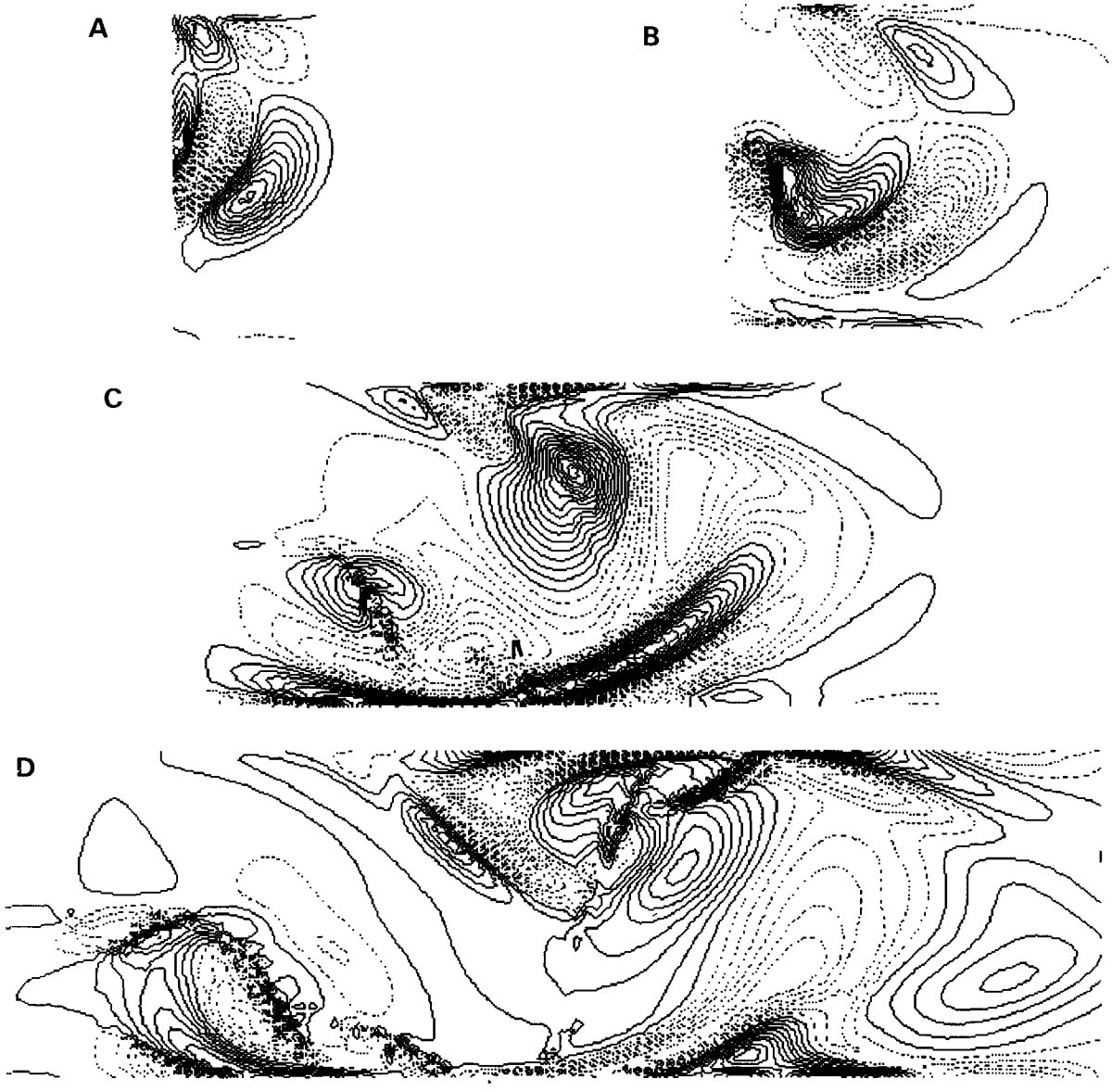

Fig. 5. Equal vorticity counters of the third velocity mode for t =1∼110 (a) $\omega_{max} = 0.0987, \omega_{min} = -0.1832, \Delta\omega = 0.0094$, $t = 1 \sim 10$ (b) $\omega_{max} = 0.1319, \omega_{min} = -0.1233, \Delta\omega = 0.0085, t = 11 \sim 20$ (c) $\omega_{max} = 0.0691, \omega_{min} = -0.0474, \Delta\omega = 0.0039, t = 21 \sim 30$ (d) $\omega_{max} = 0.0333, \omega_{min} = -0.0274, \Delta\omega = 0.0020, t = 31 \sim 40$ (e) $\omega_{max} = 0.0218, \omega_{min} = -0.0161, \Delta\omega = 0.0013, t = 41 \sim 50$ (f) $\omega_{max} = 0.0212, \omega_{min} = -0.0161, \Delta\omega = 0.0012, t = 51 \sim 60$ (g) $\omega_{max} = 0.0176, \omega_{min} = -0.0155, \Delta\omega = 0.0011, t = 61 \sim 70$ (h) $\omega_{max} = 0.0127, \omega_{min} = -0.0133, \Delta\omega = 0.0009, t = 71 \sim 80$ (i) $\omega_{max} = 0.0095, \omega_{min} = -0.0118, \Delta\omega = 0.0007, t = 81 \sim 90$ (j) $\omega_{max} = 0.0105, \omega_{min} = -0.0061, \Delta\omega = 0.0006, t = 91 \sim 100$ (k) $\omega_{max} = 0.0068, \omega_{min} = -0.0095, \Delta\omega = 0.0005, t = 101 \sim 110$

the first basis and the energy contained in the higher modes decreases very rapidly. It is interesting to see from Fig. 2a that the energy curves of the first two bases are wavy as flow develops, which is caused by the hydrodynamics instability waves contained in these modes, and between the first and the second basis there is a clear complementary relationship. But, as in Fig. 2b, the energy curves of

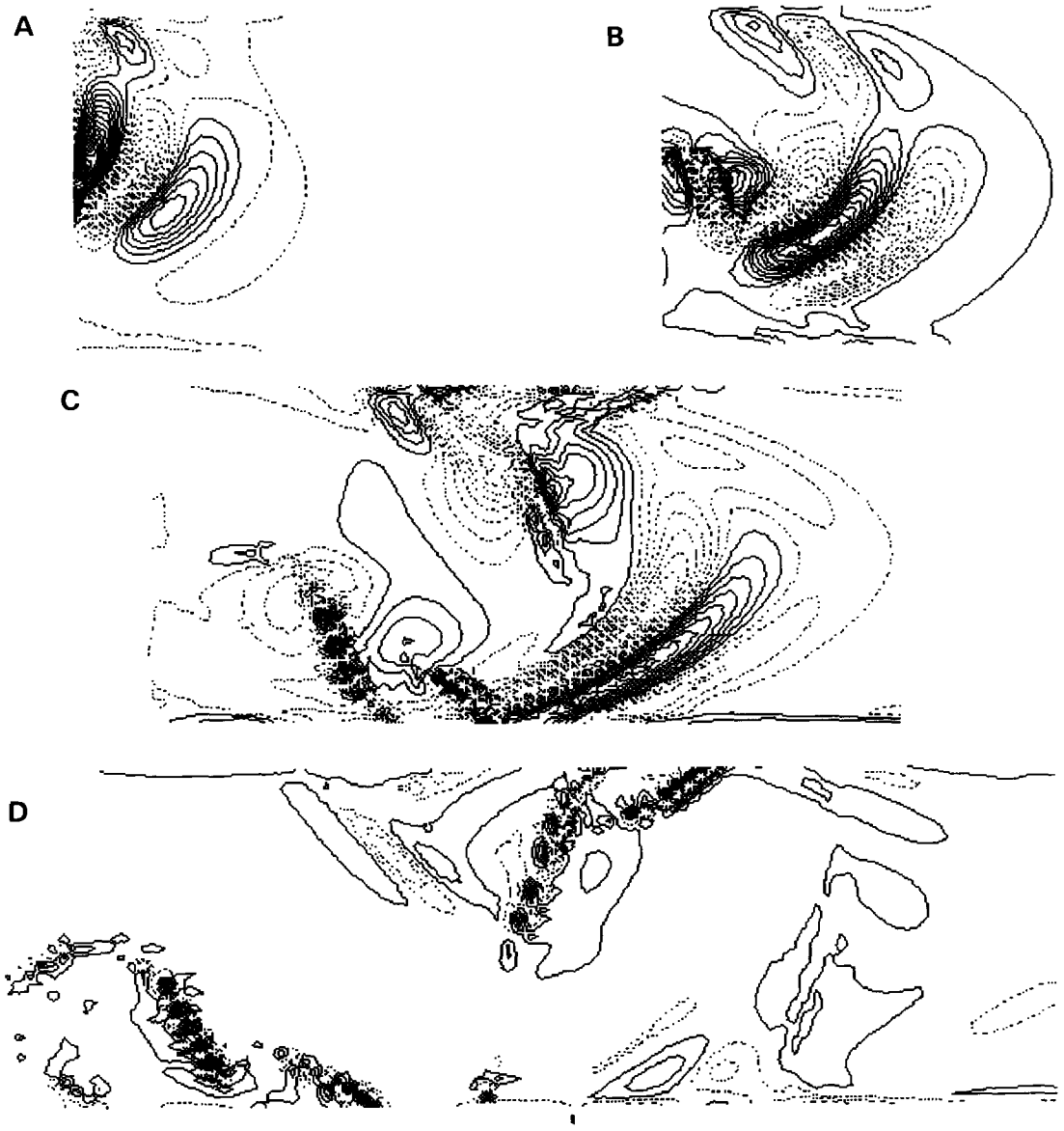

Fig. 6. Equal vorticity counters of the fourth velocity mode for t =1∼110 (a) $\omega_{max} = 0.2503, \omega_{min} = -0.1581, \Delta\omega = 0.0136, t = 1 \sim 10$ (b) $\omega_{max} = 0.0361, \omega_{min} = -0.0491, \Delta\omega = 0.0028, t = 11 \sim 20$ (c) $\omega_{max} = 0.0207, \omega_{min} = -0.0168, \Delta\omega = 0.0013, t = 21 \sim 30$ (d) $\omega_{max} = 0.0073, \omega_{min} = -0.0067, \Delta\omega = 0.0005, t = 31 \sim 40$ (e) $\omega_{max} = 0.0045, \omega_{min} = -0.0056, \Delta\omega = 0.0003, t = 41 \sim 50$ (f) $\omega_{max} = 0.0042, \omega_{min} = -0.0043, \Delta\omega = 0.0003, t = 51 \sim 60$ (g) $\omega_{max} = 0.0048, \omega_{min} = -0.0028, \Delta\omega = 0.0003, t = 61 \sim 70$ (h) $\omega_{max} = 0.0045, \omega_{min} = -0.0037, \Delta\omega = 0.0003, t = 71 \sim 80$ (i) $\omega_{max} = 0.0030, \omega_{min} = -0.0049, \Delta\omega = 0.0003, t = 81 \sim 90$ (j) $\omega_{max} = 0.0037, \omega_{min} = -0.0024, \Delta\omega = 0.0002, t = 91 \sim 100$ (k) $\omega_{max} = 0.0037, \omega_{min} = -0.0029, \Delta\omega = 0.0002, t = 101 \sim 110$

the vorticity bases vary with time smoothly and monotonically. The mechanism of this phenomenon needs further investigation.

The time histories of the spatial structures of vorticity of the first four velocity modes are shown in Fig. 3∼6 (in the figures $\triangle\omega$ are the differences between equal vorticity contours) From Fig. 3, it

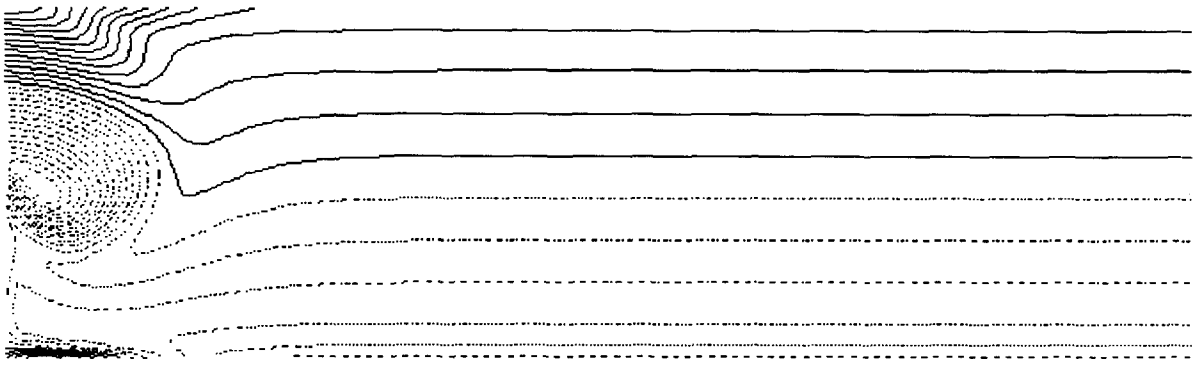

Fig. 7. Vorticity field of the step flow at t =10. ω_{max} = 0.6040, ω_{min} = −0.5912, $\Delta\omega$ = 0.0398

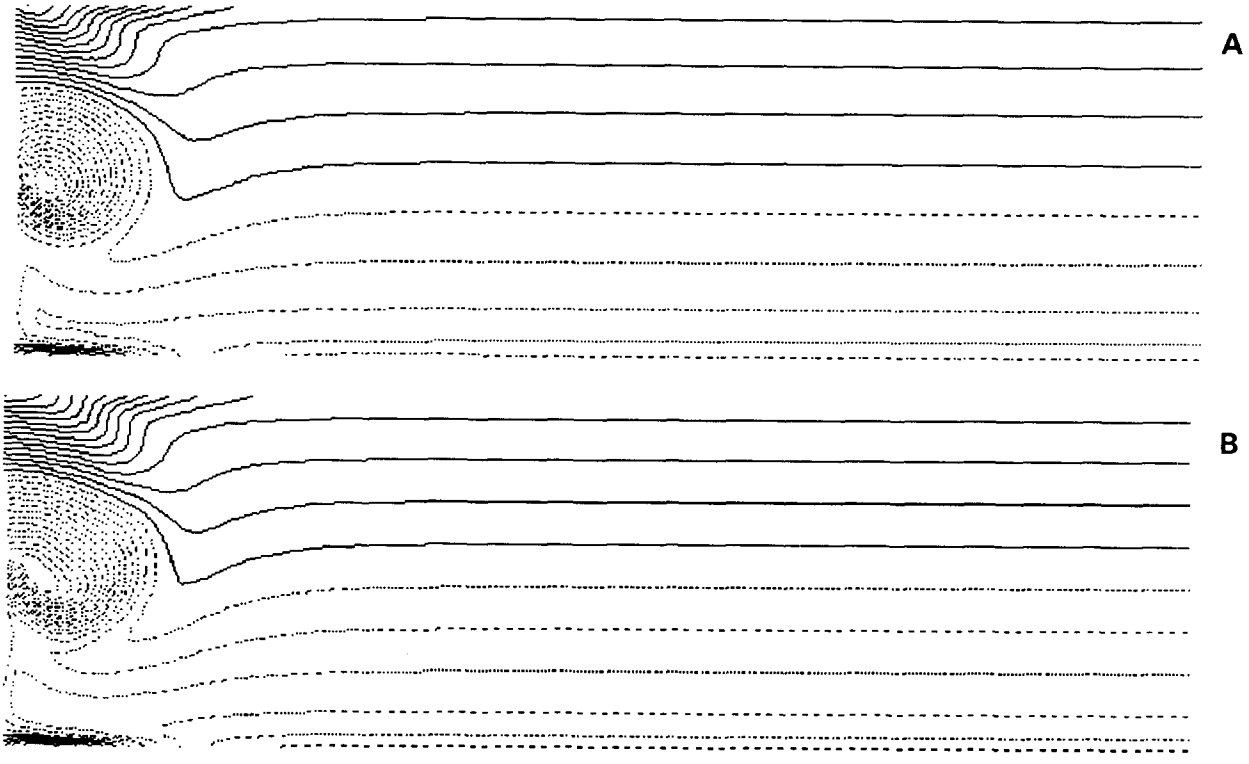

Fig. 8. Approx. vorticity fields of the step flow with velocity modes at t =10. (a) First approx., ω_{max} = 0.6428, ω_{min} = −0.7447, $\Delta\omega$ = 0.0463 (b) Fifth approx., ω_{max} = 0.6017, ω_{min} = −0.5866, $\Delta\omega$ = 0.0396

is clear that the first mode has captured the main character of the flow, i.e., the vortex slipped from the tip of the back corner of the step and moved to the exit. At the strong unsteady starting stage, the spatial structure of the first basis evolves rapidly, but at the quasi-steady stage, the structure has only little change as time pass by. The other modes represent some less significant features of the flow, and the energy contained in those modes also reduces subsequently. But it is surprised to see that the maximum vorticity in each mode is not reduced with the order; for example, the maximum

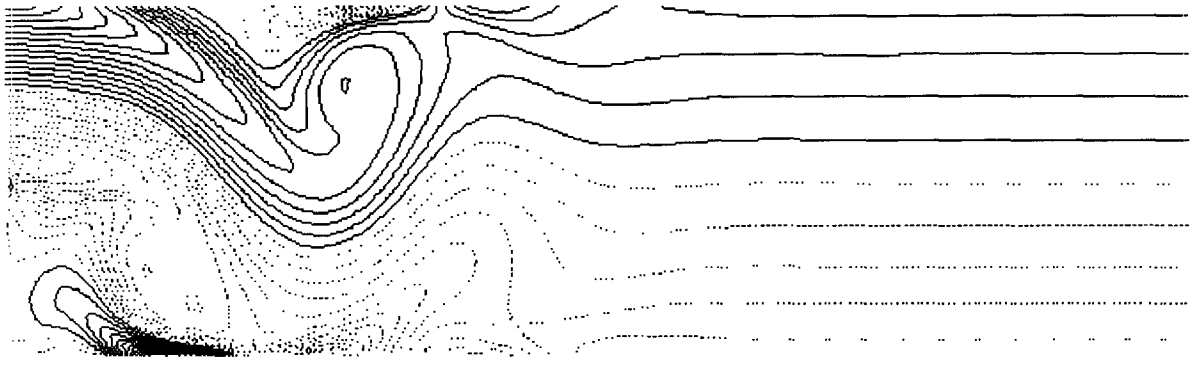

Fig. 9. Vorticity field of the step flow at t =110. $\omega_{max} = 0.6360, \omega_{min} = -0.5983, \Delta\omega = 0.0411$

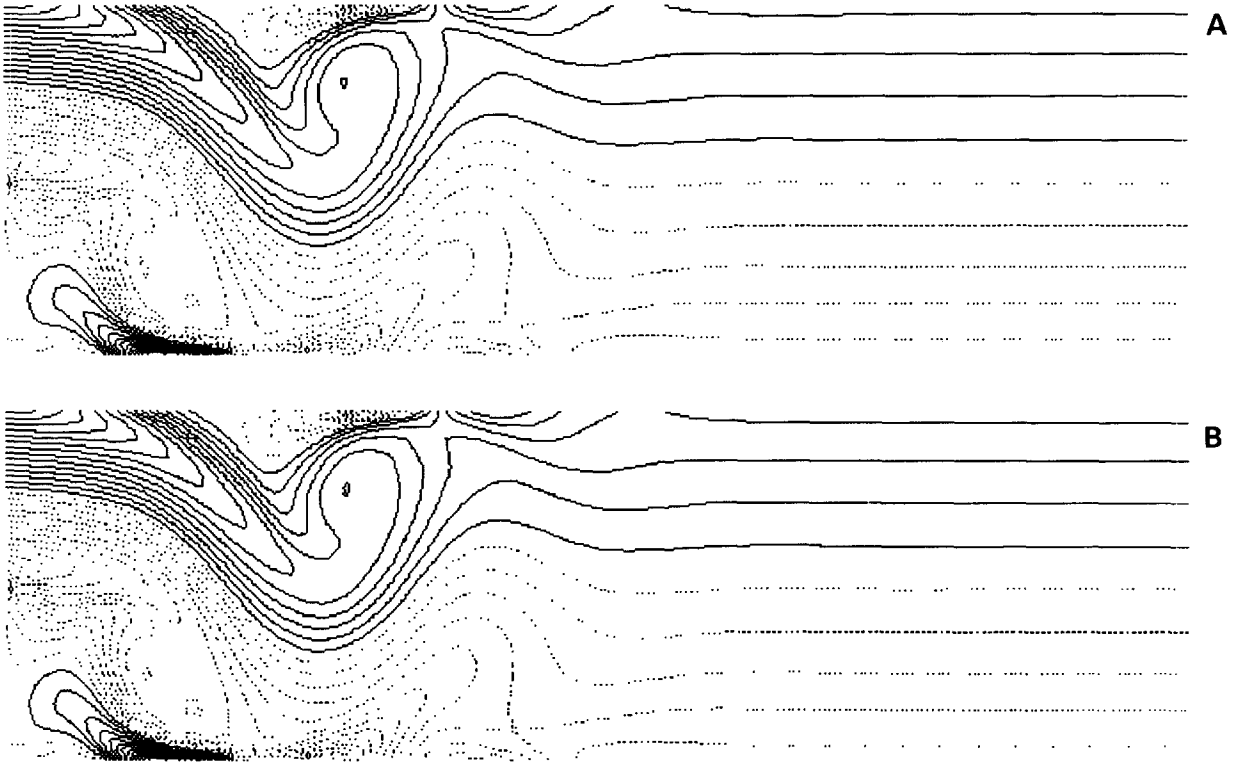

Fig. 10. Approx. vorticity fields of the step flow with velocity modes at t =110. (a) First approx., $\omega_{max} = 0.6377, \omega_{min} = -0.6003, \Delta\omega = 0.0413$ (b) Third approx., $\omega_{max} = 0.6362, \omega_{min} = -0.5981, \Delta\omega = 0.0411$

vorticity in the fourth mode (Fig. 6a) is larger than that of the third one (Fig. 5a) From these figures, the higher modes are found to correspond to some smaller and weaker vortices in the flow, which dissipate quickly as the flow approaches the steady state. At the same time section, in the spatial structures there is a kind of cancellation relation among modes. For the optimal vorticity bases, they also have similar features.

Compared with the real vorticity field of the flow at t = 10 (Fig. 7), the approximated vorticity

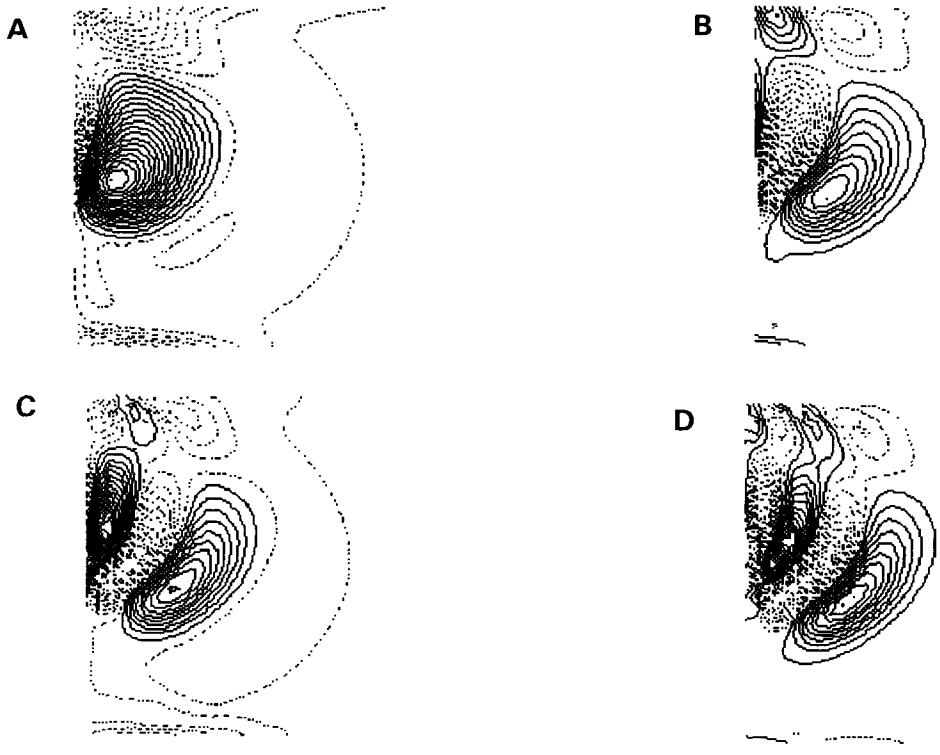

Fig. 11. Equal vorticity counters of the first four vorticity modes for t =1∼10 (a) First mode, ω_{max} = 0.7645, ω_{min} = −0.4142, $\Delta\omega$ = 0.0393 (b) Second mode, ω_{max} = 0.2563, ω_{min} = −0.5443, $\Delta\omega$ = 0.0267 (c) Third mode, ω_{max} = 0.2498, ω_{min} = −0.1365, $\Delta\omega$ = 0.0129 (d) Fourth mode, ω_{max} = 0.0843, ω_{min} = −0.0999, $\Delta\omega$ = 0.0061

fields based on the first mode and the first five modes are shown in Figs. 8a and 8b, respectively. It is clear that using the optimal modes, we have not only almost completely captured the global structures of the flow field, but also accurately represent its local features. For t = 110, Fig. 9 and Fig. 10 show the real vorticity field and the first and the first three modes' approximations, respectively. At this time only very few modes are needed to accurately approach the real flow field.

3.3.2. The optimal vorticity bases

The late fluid mechanics professor Lu Si-jia(1984) pointed out:"The essence of fluid motion is vortices." Thus if we correctly understand the mechanisms of vortex motions, then we will to a great extent hold the key to flow. Next, we take vorticity as the variable of systems, the "energy" here will be the enstrophy of the vorticity field. Again only the time-varying parts will be taken into account.

The analysis of the optimal vorticity bases of the strong unsteady flow field at the starting stage has shown that the first mode can hold 75% total enstrophy of the flow, and with the first four modes more than 99.68% total enstrophy can be captured. This result shows that the convergence rate of the optimal vorticity modes is also very fast, but compared with the optimal velocity bases, the distribution of enstrophy has a tendency to the higher modes, which is in agreement with the work of Sirovich (1991) It should be realized that this is not always the case.

At t = 100 ∼ 110, it is found that for quasi-steady flow, with just the first mode we capture 99.51%

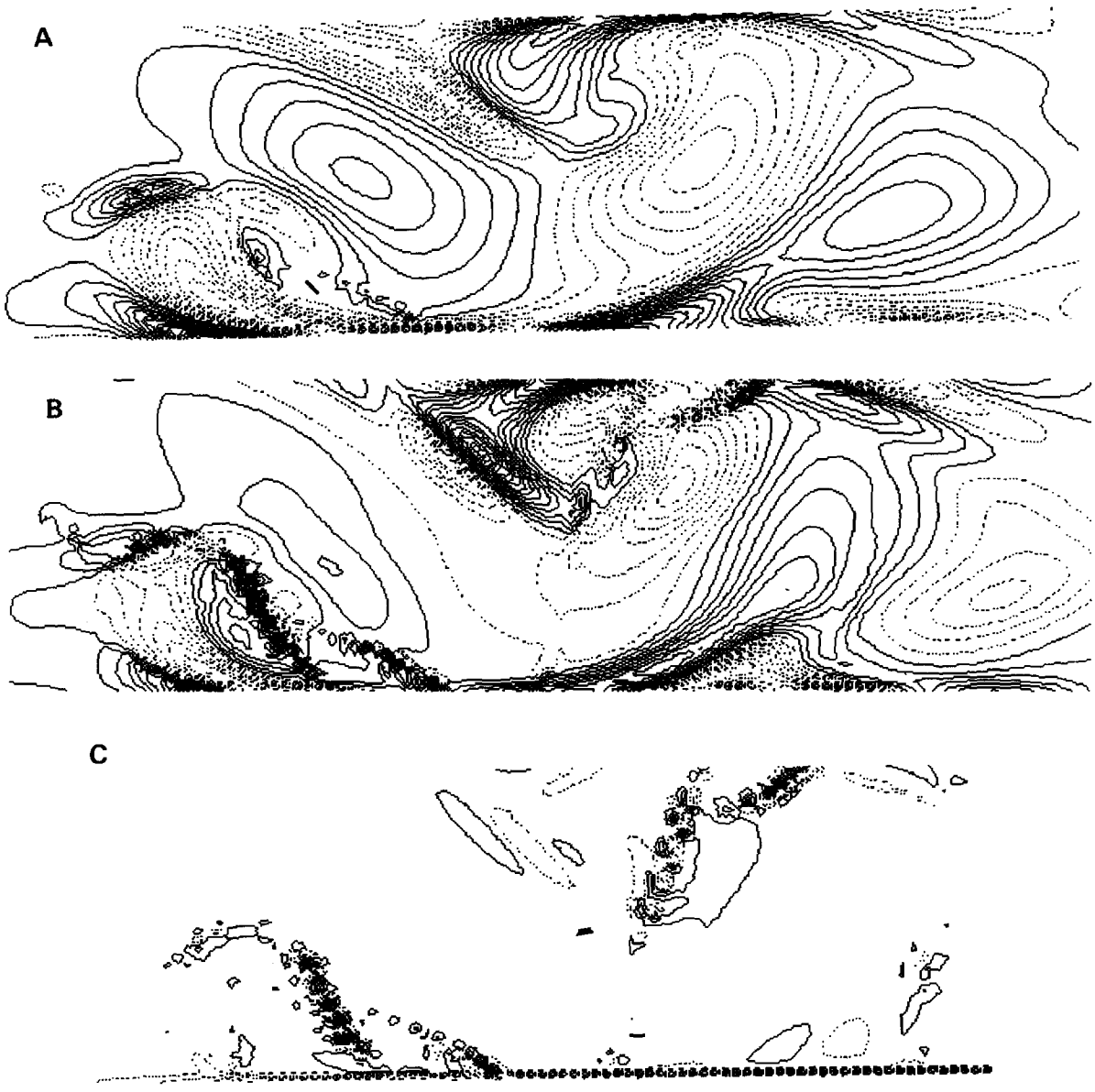

Fig. 12. Equal vorticity counters of the first three vorticity modes for t =100~110 (a) First mode, $\omega_{max} = 0.1283, \omega_{min} = -0.0881, \Delta\omega = 0.0072$ (b) Second mode, $\omega_{max} = 0.0097, \omega_{min} = -0.0064, \Delta\omega = 0.0006$ (c) Third mode, $\omega_{max} = 0.0012, \omega_{min} = -0.0018, \Delta\omega = 0.0001$

of the total enstrophy. This time the distribution of enstrophy does not approach the higher modes, but is concentrated in the lower modes; this is just opposite to the strong unsteady situation.

Figs. 11 and 12 are the vorticity field of the first four and the first three modes, for $t = 1 \sim 10$ and $t = 100 \sim 110$, respectively. Their characters are almost the same as that of the velocity bases. This shows that the vortices take the forms of highly correlated fluid energy. Fig. 13 is the approximated vorticity field based on the first mode and the first five modes for $t = 10$, and the approximated

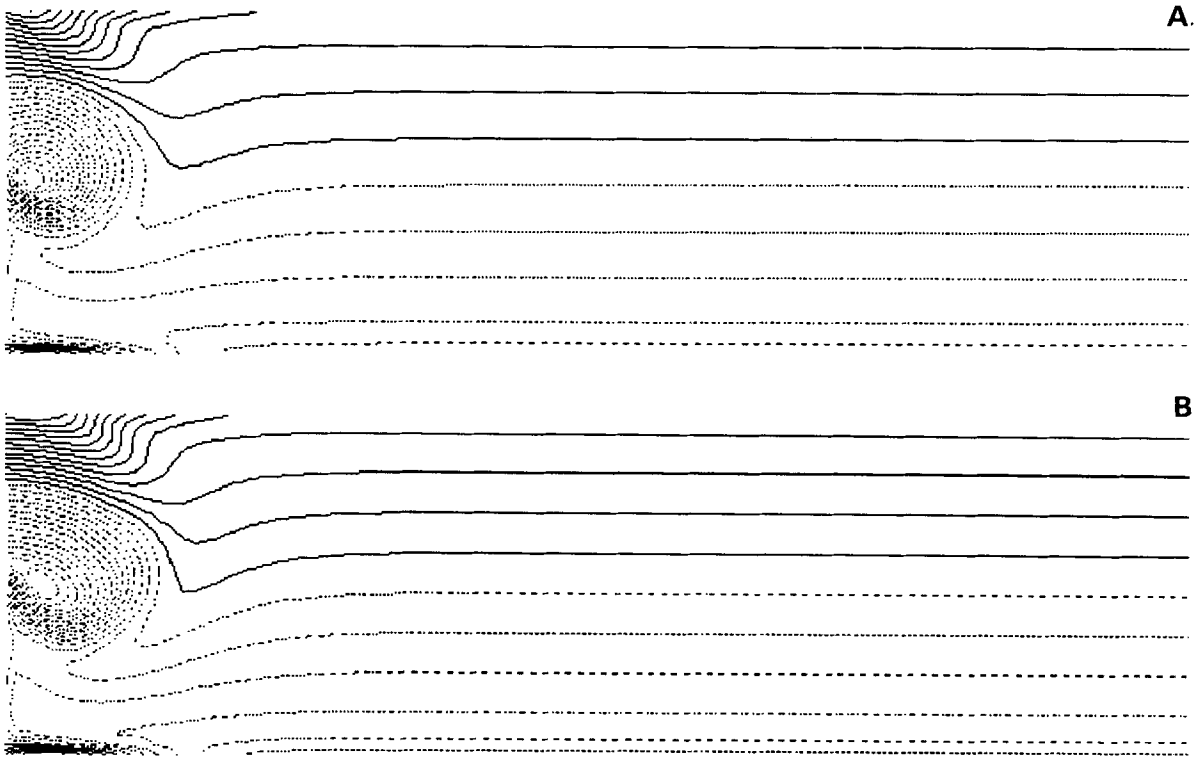

Fig. 13. Approx. vorticity fields of the step flow with vorticity modes at t =10. (a) First approx., $\omega_{max} = 0.5798, \omega_{min} = -0.7261, \Delta\omega = 0.0435$ (b) Fifth approx., $\omega_{max} = 0.5348, \omega_{min} = -0.5944, \Delta\omega = 0.0376$

vorticity fields based on the first mode and the first three modes are represented in Fig. 14, from which it can be seen that with the optimal vorticity modes, the real flow field can be approached with sufficient accuracy. As with the velocity bases, using the optimal vorticity bases to represent the flow field can also achieve very high precision. For example, at $t = 110$, with the first three vorticity modes the errors of the maximum and minimum vorticity of the approximated vorticity field to the real field are 0.002% and 0.0004%, respectively. Therefore we believe that for steady or quasi-steady flow fields, the optimal vorticity bases will be more advantageous than the velocity ones.

It should be keep in mind that the simulations are restricted to two-dimensional ones, where the vortex lines cannot be stretched and the energy cannot be transferred in the third direction; therefore the vorticity and velocity modes are closely tied together, and have a similar evolution tendency.

4. Concluding remarks

Under the global inner product optimal condition, the new theory is completely equivalent to the POD. Furthermore, with the help of the Sobolev embedding theorem the new theory has the potential to extract the local structures with specific emphases, when certain reasonable optimal conditions are adopted.

The time histories of velocity and vorticity show that as the flow approaches the steady state,

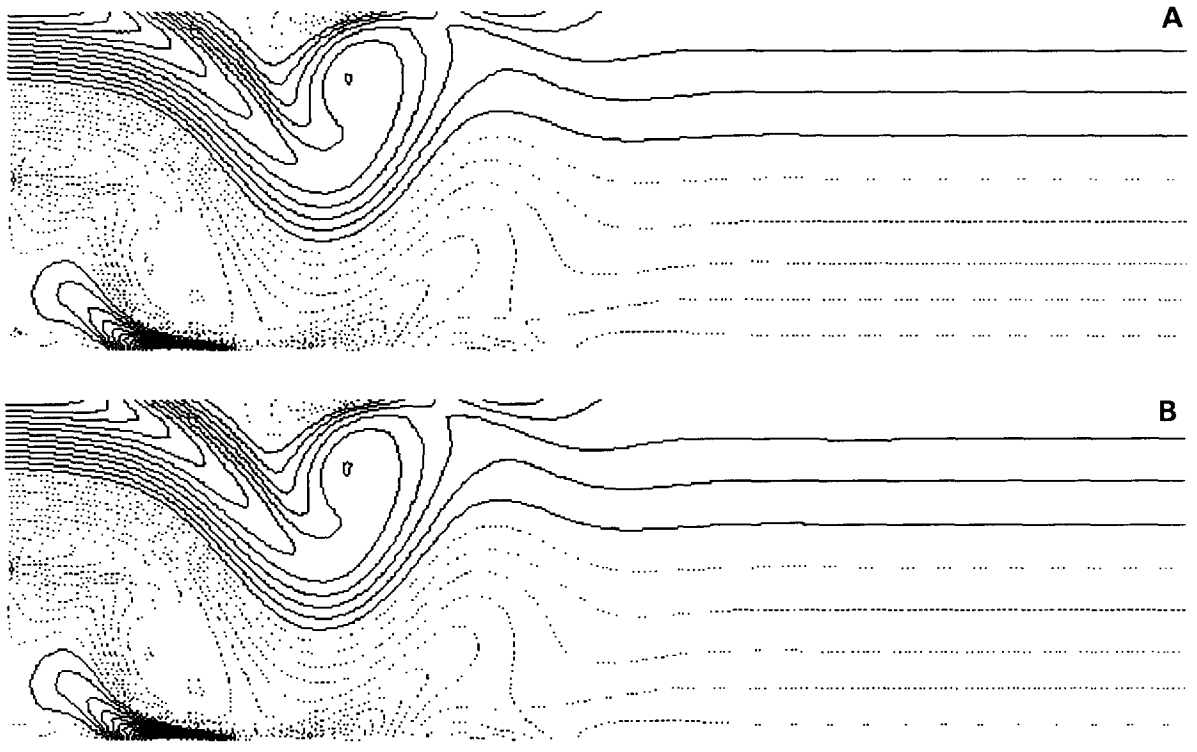

Fig. 14. Approx. vorticity fields of the step flow with vorticity modes at t =110. (a) First approx., $\omega_{max} = 0.6377, \omega_{min} = -0.6003, \Delta\omega = 0.0412$ (b) Third approx., $\omega_{max} = 0.6360, \omega_{min} = -0.5983, \Delta\omega = 0.0411$

the kinetic energy or enstrophy tends toward the leading modes, and the higher modes(i.e., small structures of the flow) decay very fast; therefore they are negligible in the simulation.

For different flows different optimal conditions should be used to extract the typical features. For low Reynolds number quasi-steady vortex flows, taking vorticity and enstrophy as the variable and the optimal condition respectively can efficiently capture the primarily structures of the flows. But this cannot be extended to fully developed turbulent flows.

We also learn from the simulation that a large fraction of the fluctuation enstrophy is carried by the first few modes; hence, in two-dimensional vortical flows, the flow structures carrying most enstrophy of the flow can represent the main features of the flow.

Acknowledgements

Financial support from LNM, Institute of Mechanics, Academia Sinica of China during the periods from 1992 to 1994, and from the National Natural Science Foundation of China # 19472077 is gratefully acknowledged. The invaluable comments of the referees are also greatly appreciated.

References

Adams, R. (1975) *Sobolev Space* (Academic, New York).

Berkooz, G., P. Holmes and J.L. Lumley (1993) The proper orthogonal decomposition in the analysis of turbulent flows, *Annu. Rev. Fluid Mech. 25*, 539–575.

D.K. Gartling (1990) A test problem for outflow boundary conditions-flow over a backward-facing step, *Inter. J. Num. Methods Fluids 11*, 953–967.

Glezer, A., Z. Kadioglu and A.J. Pearlstein (1989) Development of an extended proper orthogonal decomposition and its application to a time periodically forced plane mixing layer, *Phys. Fluids A 1*, 1363–1373.

Gresho, P.M. and R.L. Sani (1990) Introducing four benchmark solutions, *Inter. J. Num. Methods Fluids 11*, 951–952.

Kirby, M. (1992) Minimal dynamical systems from PDEs using Sobolev eigenfunctions, *Physica D 57* 466–475.

Lumley, J.L. (1967) The structure of inhomogeneous turbulent flows, in: *Atmospheric Turbulence and Radio Wave Propagation*, eds. A.M. Yaglom and V.I. Tatarski (Moscow, Nauka) 166–178.

Schmidt, E. (1907) Zur Theorie der linearen und nichtlinearen Integralgleichungen. I Teil: Entwicklung willkülicher Funktion nach Systemen vorgeschriebner, *Mathematische Annalen 63*, 433–476.

Sirovich, L. (1987) Turbulence and the dynamics of coherent structures, *Quart. Appl. Math XLV*, 561–590.

Sirovich, L. (1991) Empirical eigenfunctions and low dimensional system, in: *New Perspective in Turbulence*, ed. L. Sirovich (Springer,Berlin) 139–163.

Wu, C.J. and H.S. Shi (1994) Advance in Flow Database Analysis and Construction of Low-Dimensional Dynamical Systems, *J. Hydro. A, 9*(6), 716–723 (in Chinese).

Ye, Q.K. and Z.M. Wang (1986) *Computational Method in Optimization and Optimal Control* (Science Press).